Fermilab FERMILAB-TM-2134 November 2000

Dynamic Aperture of the Recycler Ring

Meiqin Xiao and Tanaji Sen
Fermi National Accelerator Laboratory
P.O. Box 500
Batavia, IL 60510

1 Introduction

This report describes the dynamic aperture tracking for the Recycler Ring [1] based on the latest modified lattice *Ver 20*. The purpose of the calculation is to check the optical properties of the lattice with the replacement of the high beta straight section ($HB30$) by a low beta straight section ($LB30$) for stochastic cooling.

2 Tracking code, lattice and magnetic field errors

The code used for the tracking is MAD ($Ver8.16$). Magnetic field errors can be characterized in terms of coefficients (b_n, a_n) in a multipole expansion of the magnetic field,

$$B_y + iB_x = B_0 \sum_{n=0}^{\infty} (b_n + ia_n)(\frac{x+iy}{r})^n \tag{1}$$

where b_0, b_1, b_2, . . ., are the normal dipole, quadruple, sextupole, . . ., field components, a_0, a_1, a_2, . . ., are the corresponding skew components and r is the reference radius at which the multipole components are measured. In the bare recycler lattice of *Version 20*, the design angle and measured b_1 and b_2 are included in the gradient magnet named G_{body} (see the beam line defined in Appendix A), and the measured normal quadrupole component b_1 is reflected in the main quadrupole named Q_{body}. All other high order multipole components of each magnet are treated in the lattice as two thin lenses, placed at the entrance and the exit of the magnet respectively. The measured dipole error b_0 is treated in the lattice as an EFIELD element.

The field errors, represented by field coefficients b_n, a_n, are extracted from field harmonic measurements at a radius of 1 inch (2.54cm). These coefficients multiplied by 10,000 equal a single unit in the tables supplied by the magnet measurement group, i.e.

$$(b_n^F, a_n^F) \quad \text{Fermilab Units} = (b_n, a_n) \times 10^4 \tag{2}$$

However, the strength of a multipole K_n in MAD[2] is defined as

$$K_n = \frac{B^{(n)}}{P_0/e} = \frac{B^{(n)}}{B\rho} \tag{3}$$

Thus, the integrated strengths of thin multipole elements are converted from the multipole components in Fermilab units to MAD units as follows:

$$(KN_n, KS_n)\frac{L}{2} = 10^{-4} \times (b_n^F, a_n^F) \cdot n! \frac{B_0/(B\rho)}{r^n}\frac{L}{2} \tag{4}$$

for normal and skew components KN_n, KS_n where L is the magnet length, B_0 is the reference field, r = 1"=$0.0254m$ and ($B\rho$) is the magnetic rigidity. The energy of the Recycler Ring is taken as 8 GeV. The momentum and rigidity are

$$P_0c = \sqrt{W(2E_0 + W)} = 8.889GeV\ , \qquad (B\rho) = \frac{P_0c}{ec} = 29.650\text{Tesla} \cdot \text{m} \tag{5}$$

3 Optics of the lattices with high beta and low beta straight sections

The high beta straight section ($HB30$) will soon be replaced by a low beta section ($LB30$) for stochastic cooling in the Recycler Ring. The optical calculation is based on the lattice with a low beta section ($LB30$)($Ver2.0$), designed by W. Wan. For the purpose of comparison, the calculation for the lattice with the high beta section ($HB30$) has also been done. Figures 1 and 2 show the beta functions in the high beta and low beta lattice respectively. The significant differences are of course in the cooling insertion. Compared to maximum beta values of $(\beta_x, \beta_y) = (242, 278)$m in the $HB30$ lattice, the low beta version $LB30$ has maximum values of (71,56)m, roughly factors of 3-5 lower. To first order in multipole strength,

$$\text{Resonance driving terms } \propto \beta_x^{m/2}\beta_y^{(n-m)/2}(b_n, a_n)\ , \qquad m = 0, \ldots, n$$

The tune shift with amplitude terms are also smaller when the beta functions are reduced. We therefore expect that the low beta lattice will have a higher dynamic aperture than the high beta lattice. This report will quantitatively estimate the difference in the theoretical dynamic aperture.

We observe that there is some beta beating in the arcs in both lattices, as seen in Figures 1 and 2. Since we use the measured values of the quadrupole gradients (as opposed to the ideal values) in our lattice descriptions, there is a beta beat. Retuning the quadrupoles, especially those in the phase trombone, could reduce this beating and possibly increase the dynamic aperture.

The low beta lattice $LB30$ has fractional tunes closer to the desired values (0.425, 0.415). The integer part of the tune in the x - plane in this lattice is one integer larger than the high beta lattice $HB30$. Compared to the bare lattice, the tune shifts resulting from the changes in closed orbit due to dipole field errors and all the other high order multipole components (except sextupole components) are quite small, $\Delta\nu_x = 0.00076, \Delta\nu_y = 0.000376$. A summary of the optical parameters of the two lattices is shown in Tables 2 and 3 in Appendix B.

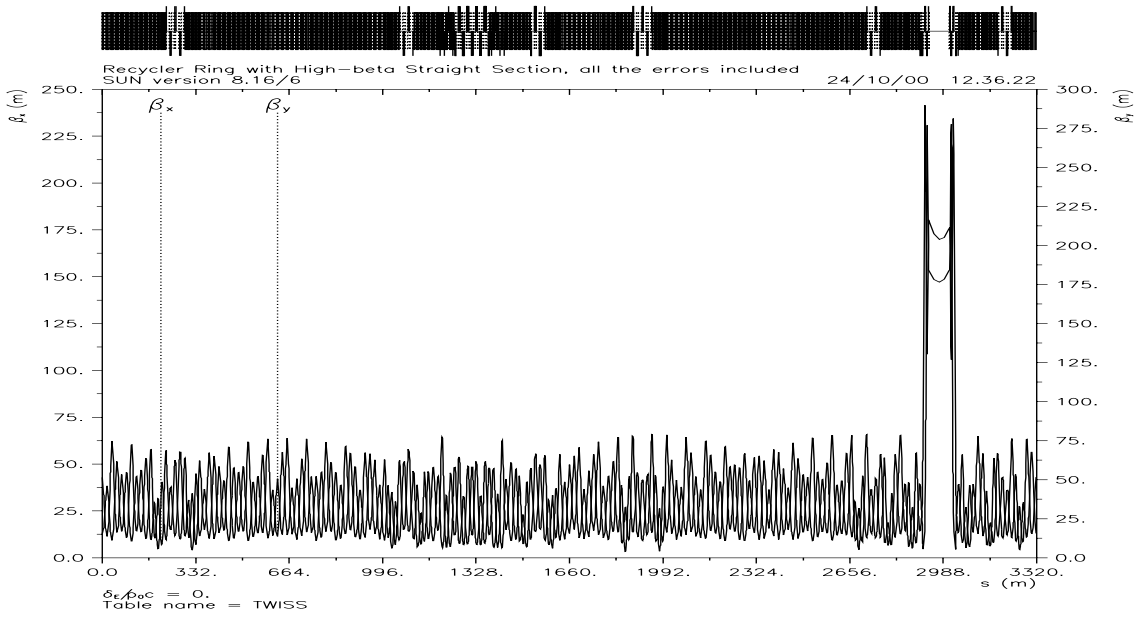

Figure 1: Beta functions in the high beta lattice $HB30$.

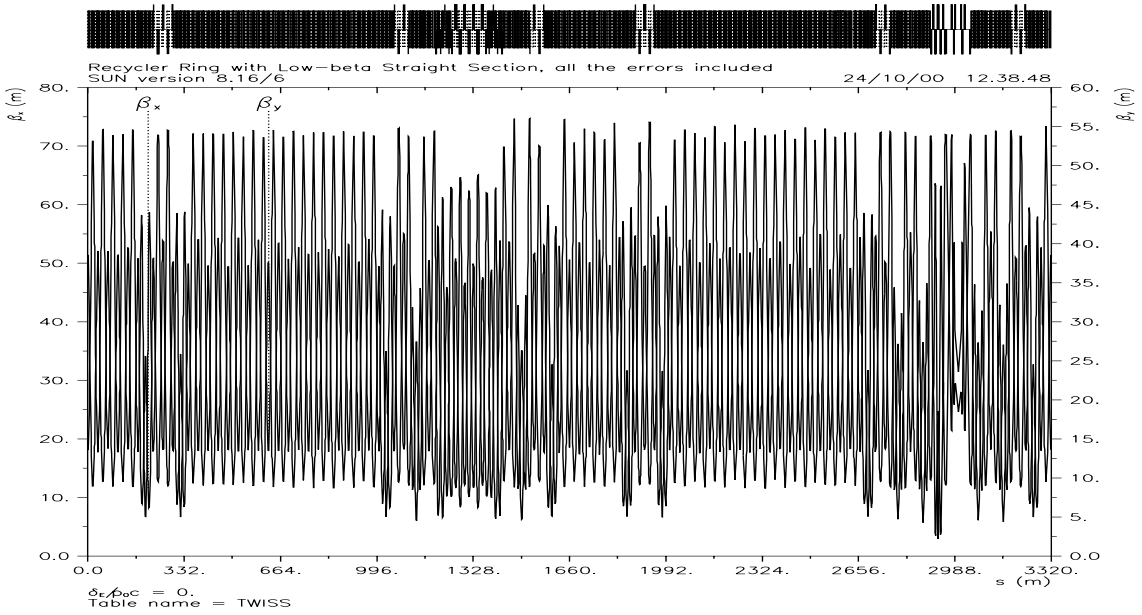

Figure 2: Beta functions in the low beta lattice $LB30$.

It was found in tracking simulations that treating each combined function magnet as a thick element with a single thin lens nonlinearity at the center is incorrect. For instance the dipoles in the arc cells are 3.099 meters long and those in the dispersion cells are 4.496 meters long. For reasons to be explained in Section 5 these magnets need to be divided into several slices. The optical results after splitting the gradient magnets into 16 pieces for the lattices with $HB30$ and $LB30$ are listed in Tables 2 and 3 respectively. From the tables we can see that there are no significant differences in the linear optical functions with and without splitting. There are however significant differences in the nonlinear behaviour as a consequence of the splitting.

4 Dynamic aperture tracking

Stability of particles in the Recycler Ring is tested by launching an array of particles at different amplitudes in the presence of magnetic field errors described in Section 2. The misalignments of the ring have not been included in the tracking simulations. We do not need to use the phase trombone to adjust the tunes since the tune shifts due to the field errors are small enough.

Chromaticity sextupoles are used to correct the linear chromaticities to the designed value $\nu_x^{'}$ = -2.0, $\nu_y^{'}$ = -2.0. Sextupoles are placed in the arc cells where the dispersion is non zero. In the Recycler Ring, there are 8 and 16 sextupoles for chromaticity correction in the horizontal and vertical plane respectively. The strengths (in units of m^{-3}) of the linear chromaticity correcting sextupoles can be found approximately from the following expressions[3]

$$k2_F = \frac{4\pi}{L_F N_{SF} D_x^{max}(\beta_x^{max}\beta_y^{max} - \beta_x^{min}\beta_y^{min})}\{[C_x - C_x^{latt}]\beta_y^{max} + [C_y - C_y^{latt}]\beta_x^{min}\} \quad (6)$$

$$k2_D = \frac{4\pi}{L_D N_{SD} D_x^{min}(\beta_x^{max}\beta_y^{max} - \beta_x^{min}\beta_y^{min})}\{[C_x - C_x^{latt}]\beta_y^{min} + [C_y - C_y^{latt}]\beta_x^{max}\} \quad (7)$$

where L_F and L_D are the lengths of the sextupoles. N_{SF} and N_{SD} are the numbers of cells with sextupoles in the horizontal and vertical planes. The minimum and maximum Twiss functions β_x, β_y and D_x refer to the extreme values in a cell. C_x and C_y are the corrected values of the linear chromaticity, typically set to -2 in both planes while C_x^{latt} and C_x^{latt} are the uncorrected linear chromaticities of the lattice. The HARMON module in MAD can be used to adjust the strengths of the sextupoles to correct linear chromaticity. Setting the initial values of the strengths of the sextupoles in the lattice to the values obtained from Eq.(6) and Eq.(7), we get the corrected chromaticities $\nu_x^{'}$ = -2.000 and $\nu_y^{'}$= -2.000 when the strengths of sextupoles are $k2_F = 0.2627$ and $k2_D = -0.2794$.

The normalized 95% emittances ϵ_{xn} and ϵ_{yn}, are $18\pi mm.mrad$ in both planes. The lattice description begins with the cell $HC328$ in the Recycler Ring and the beam sizes at this point are

$$\sigma_{x0} = \sqrt{\frac{\beta_x \epsilon_{xn}}{(\beta\gamma)\cdot 6\pi}}, \quad \sigma_{y0} = \sqrt{\frac{\beta_y \epsilon_{yn}}{(\beta\gamma)\cdot 6\pi}}, \quad \sigma = \sqrt{\sigma_{x0}^2 + \sigma_{y0}^2} \quad (8)$$

Particles are launched with a distribution of amplitudes with neighbouring particles differing in amplitude by either $1\sigma_{x0}$ or $1\sigma_{y0}$. For each fixed x-amplitude, we search the largest y-amplitude for which the particle survives 100,000

	$\langle DA \rangle$ (units of σ)	
	High β lattice	Low β lattice
With 1 kick per magnet ($\Delta p/p = 0$)	3.0	3.0
With 16 kicks per magnet ($\Delta p/p = 0$)	9.5	16.5
With 16 kicks per magnet ($\Delta p/p = -0.003$)	-	13.0
With 16 kicks per magnet ($\Delta p/p = +0.003$)	-	9.2

Table 1: Average radial dynamic aperture calculated after tracking for 100,000 turns with the high and low beta lattices. Increasing the number of kicks to 16 per gradient magnet increases the dynamic aperture significantly. As will be argued in Section 5, this number of kicks is sufficient to assure convergence of the calculated dynamic aperture.

turns. We also check that particles with smaller y amplitudes are stable over these numbers of turns. This is repeated for several x amplitudes until the largest y-amplitude falls to zero. The dynamic aperture is then defined as the average of all the largest stable radial amplitudes, i.e.

$$\text{Dynamic Aperture} = \langle \sqrt{A_x^2 + A_y^2} \rangle$$

where A_y is the largest stable amplitude in y for a given x amplitude A_x.

Including all errors, tracking over 10,000 turns in the lattices with high beta and low beta sections shows that the dynamic apertures for both lattices are about 3σ on average, plotted in black in Figure 3 and 4. This value is much less than expected. An earlier simulation with the tracking code TEAPOT of the lattice with the high beta section showed a larger dynamic aperture [4]. By default TEAPOT splits each magnet into a number of slices whereas in MAD this needs to be explicitly specified in the lattice. To determine whether the difference between the tracking codes was due to the splitting, the lattice description in MAD was modified with each gradient magnet split into 16 pieces. Now by using MAD again, we find that the dynamic apertures are 9.5σ ($271\pi mm.mrad$) on average for the high beta lattice after both 10,000 and 100,000 turns. The dynamic apertures for the low beta lattice are 16.1σ ($778\pi mm.mrad$) on average after 10,000 turns and 16.5σ ($817\pi mm.mrad$) on average after 100,000 turn and with the chromaticity corrected in this tracking. They are plotted in red in Figure 3 and Figure 4 respectively.

The dynamic aperture for particles with constant momentum deviations of ± 0.003 are shown in Figure 4. The results are summarized in Table 1. Particles with a constant negative momentum deviation have a larger dynamic aperture than those with a positive momentum deviation. A possible explanation of this may be due to the tune dependence on amplitude and momentum deviation, and the resonances that are nearby. Figure 5 shows that 7th and 12th order resonances are the closest resonances. Large amplitude particles e.g. at 7σ with negative $\Delta p/p$ are in the space between skew 7th order resonances which may not be strongly driven while those with positive $\Delta p/p$ are closer to a normal 7th order resonance and several 12th order resonances.

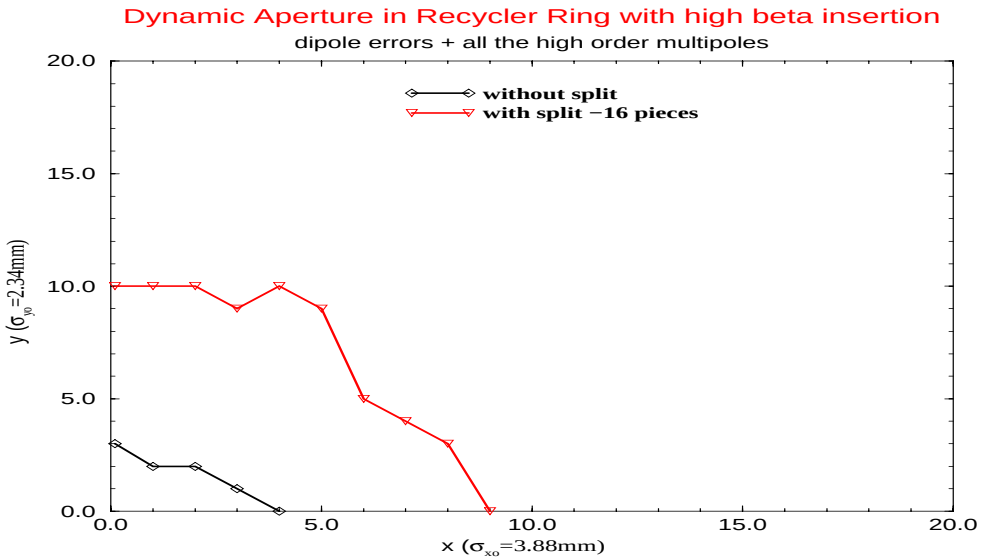

Figure 3: Dynamic aperture in Recycler Ring after 100,000 turns with the high beta insertion for two different models of the nonlinearites. In one case, there is only a single nonlinear kick at the center of each gradient magnet and in the other there are 16 kicks (keeping the integrated kick strength constant) over the length of these gradient magnets. With more kicks per magnet, the dynamic aperture is found to increase considerably.

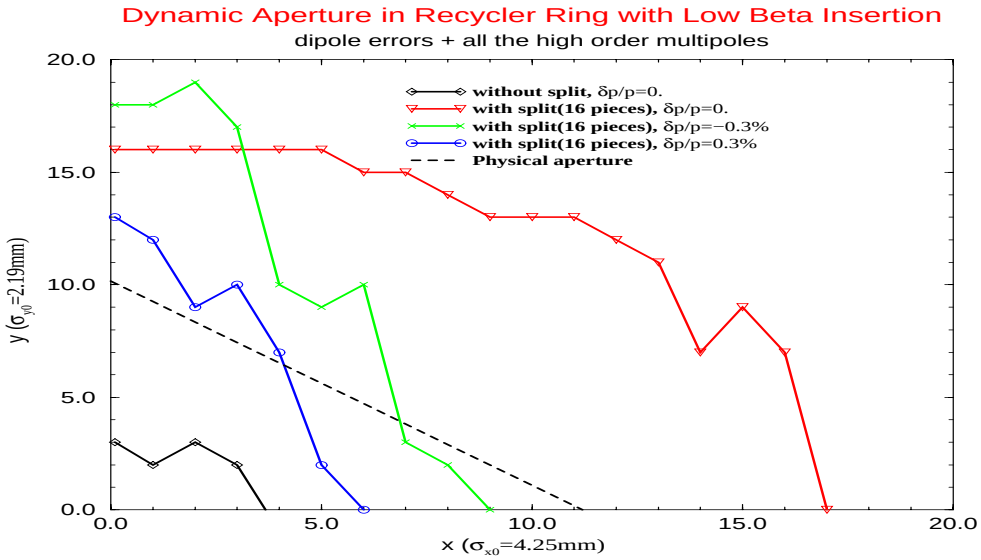

Figure 4: Dynamic Aperture in the Recycler Ring after 100,000 turns with the low beta insertion and for the same two models as in Figure 3. Also shown are the dynamic apertures for particles with constant momentum deviations of ± 0.003. The beam pipe contour (in units of the rms beam size) is drawn to illustrate the fact that in this tracking model, the dynamic aperture of particles with $\Delta p/p = 0$ exceeds the physical aperture.

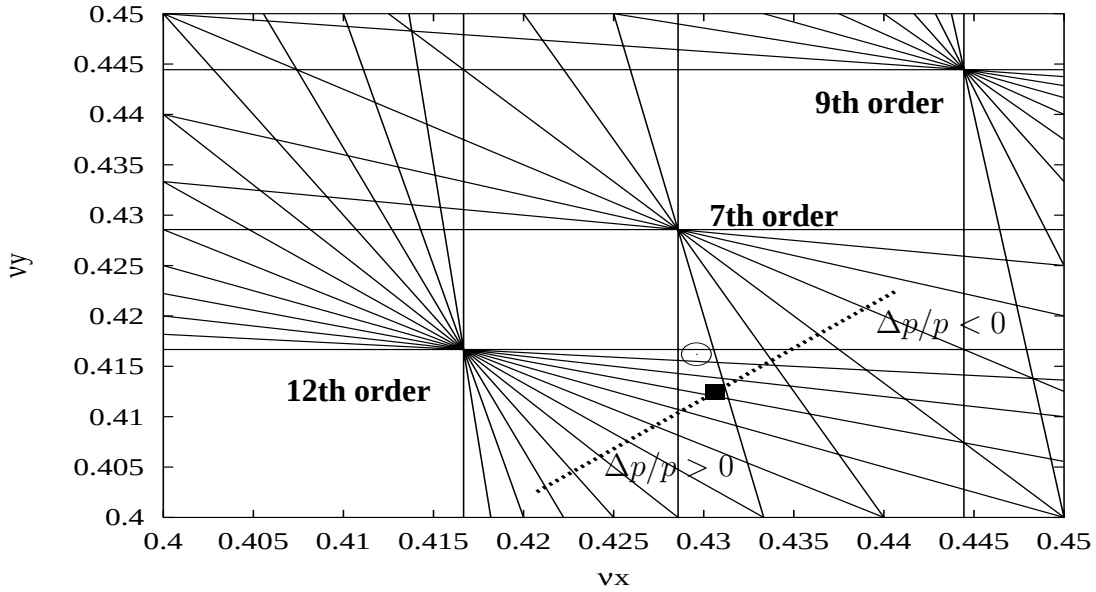

Figure 5: Resonances, the zero amplitude tune shown as an empty circle $\odot$, and the tune at an amplitude of 7σ shown as a filled box. The dotted line shows the tunes for 7σ particles with momentum deviations in the range $-0.005 \leq \Delta p/p \leq 0.005$ due to a linear chromaticity of $\nu' = -2$. Particles with $\Delta p/p < 0$ have larger tunes while those with $\Delta p/p > 0$ have smaller tunes. The closest resonances are the 7th order and 12th order resonances. Particles with $\Delta p/p < -0.004$ lie in the space between 7th order skew resonances which may not be strongly excited. Particles with $\Delta p/p > 0$ are close to the 7th order normal resonance $7\nu_x = 178$ and several 12th order resonances.

5 Analysis

The tracking results yielded a few surprises. The first surprise was that with only a single multipole kick in the center of each magnet, the dynamic aperture of both lattices was nearly the same. This result which is specific to this particular model of nonlinearities can be understood if the dynamic aperture is dominated by the nonlinear kicks from the arcs. Since the arcs have more magnets than the straight sections and the beta functions in the arcs are of the same order of magnitude as those in the straight sections for both lattices, this explanation is in the realm of being plausible but somewhat unexpected nonetheless. This explanation turns out to be wrong however when the nonlinear lattice model is changed to incorporate 16 multipole kicks, each with 1/16th of the integrated strength of the single kick in the previous model, along the length of each gradient magnet. We found that the dynamic aperture increases in this model for both lattices but the low beta lattice has the larger dynamic aperture - the result that we expected. The surprise in this model was the rather large increase in dynamic aperture when the number of kicks per magnet was increased to 16.

A possible cause of this large change in dynamic aperture could be a rapid variation in the beta function along the magnet. A single kick at the center of a magnet where the beta function is large may have a larger effect compared

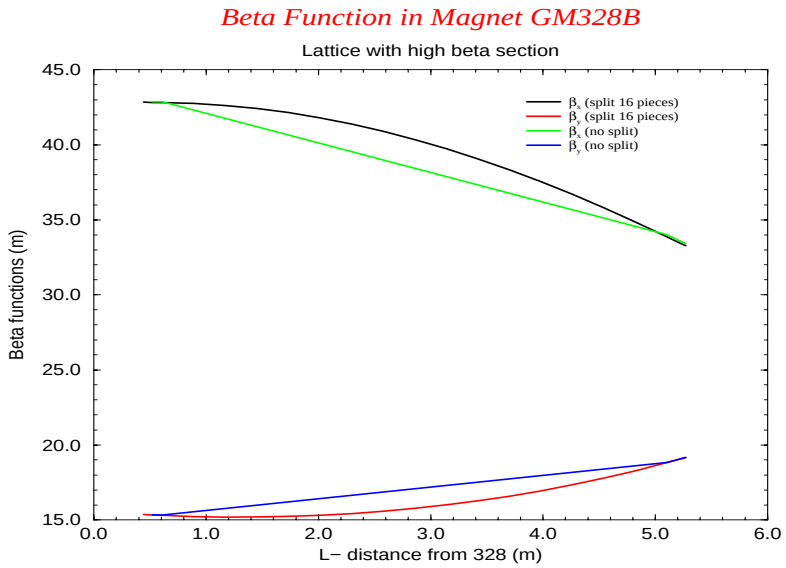

Figure 6: Beta function in Magnet GM328B shown at the two ends (no split) and also at 16 different locations within the body of the magnet.

to the case when there are several kicks at locations of smaller beta. This hypothesis was tested on a typical magnet $GM328B$ in the high beta lattice. Figure 6 shows the beta functions with and without the several splits. We observe that the beta functions are not varying rapidly along the length and furthermore the horizontal beta functions are in fact *larger* at several locations with the splits than the beta function at the center without the splits. The source of the increase in dynamic aperture therefore lies elsewhere.

The main reason (we believe) for this large change in dynamic aperture is that there is a sufficient phase advance (about 7 degrees) along the length of each gradient magnet. When there are several kicks along the length, each of these occurs at a slightly different phase. The resultant of these somewhat incoherent kicks will always be smaller than a single coherent kick which has the same strength as the sum of all the individual kicks. This is illustrated in Figure 7. This is a qualitative explanation of the effects of several incoherent kicks. A more exact calculation in Appendix C shows that the change in the linear Courant-Snyder invariant J decreases as the number of kicks is increased from 1 to 2 and based on these arguments we expect that the change in J will decrease with increasing number of kicks until we reach the asymptotic limit when the change in J remains nearly constant.

There are several ways of determining the minimum number of kicks necessary to reach the asymptotic limit. The figure of merit we choose is the tune shift with amplitude. We compare the model where the gradient magnets are split into 16 pieces with another model where the gradient magnets are split into 32 pieces and the quadrupoles are split into 4 pieces. The tune shifts are determined by tracking two groups of particles for 1024 turns. Within each group the $x$amplitude is fixed, one at $0.1\sigma_{x0}$ and the other at $10\sigma_{x0}$ respectively, while the y amplitudes are varied from $1.0\sigma_{y0}$ to $11.0\sigma_{y0}$.

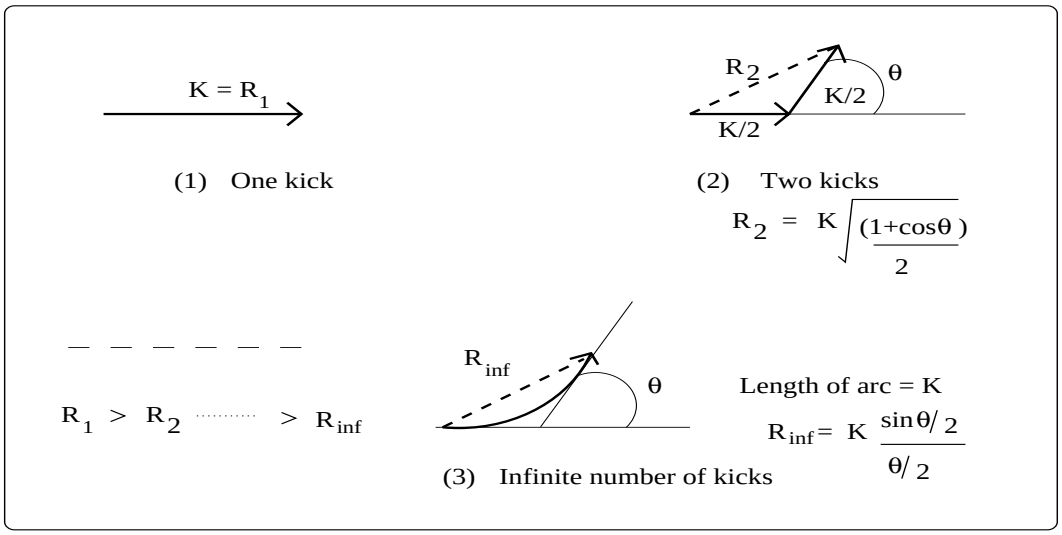

Figure 7: Resultant of several incoherent kicks. The sketch labelled (2) shows the resultant R_2 when there are two kicks, each of length $K/2$. The sketch (3) shows the resultant in the asymptotic limit of an infinite number of kicks. Here the kicks lie along the arc of a circle while the resultant R_{inf} is the chord along this arc. The resultant decreases as the number of kicks is increased while keeping the sum of the length of individual kicks constant at K and the angle between the first and last kick constant at θ, i.e. $R_1 \geq R_2 \ldots \geq R_{inf}$.

The FFT spectrum for each particle under the influence of all field errors is calculated from the tracking results. Figure 8 shows the FFT spectra for two selected particles with the same y amplitude but at two different x amplitudes. A Hanning filter is applied to improve the resolution of the tune calculation. Even though the y amplitudes of these two particles are the same, there is a significant difference in the vertical tune $\Delta\nu_y = 0.0022$ due to the large cross-detuning term $\partial\nu_y/\partial J_x$ (=$\partial\nu_x/\partial J_y$) or in words due to the dependence of the vertical tune on the horizontal amplitude. We also observe a significant signal of the horizontal tune in the vertical spectrum (and vice versa) which indicates that the coupling is non-negligible. Figure 9 shows the variation of the horizontal and vertical tune as the vertical amplitude is increased keeping the horizontal amplitude constant. We observe that the change in ν_x is larger than that in ν_y. At amplitudes $(A_x = 0.1\sigma_{x0},\ A_y \geq 11\sigma_{y0})$, ν_x approaches the 7th order resonance.

Figure 10 displays the tune difference between the lattices with two split models vs the particle amplitudes. The tune differences are within 1.4×10^{-5} which is also roughly the resolution of the tune calculation with the Hanning filter. We take this convergence in tune shifts to indicate that splitting the gradient magnets into 16 pieces suffices for the calculation of the dynamic aperture. If this required greater justification, one could examine other nonlinear features such as the smear in order to prove convergence.

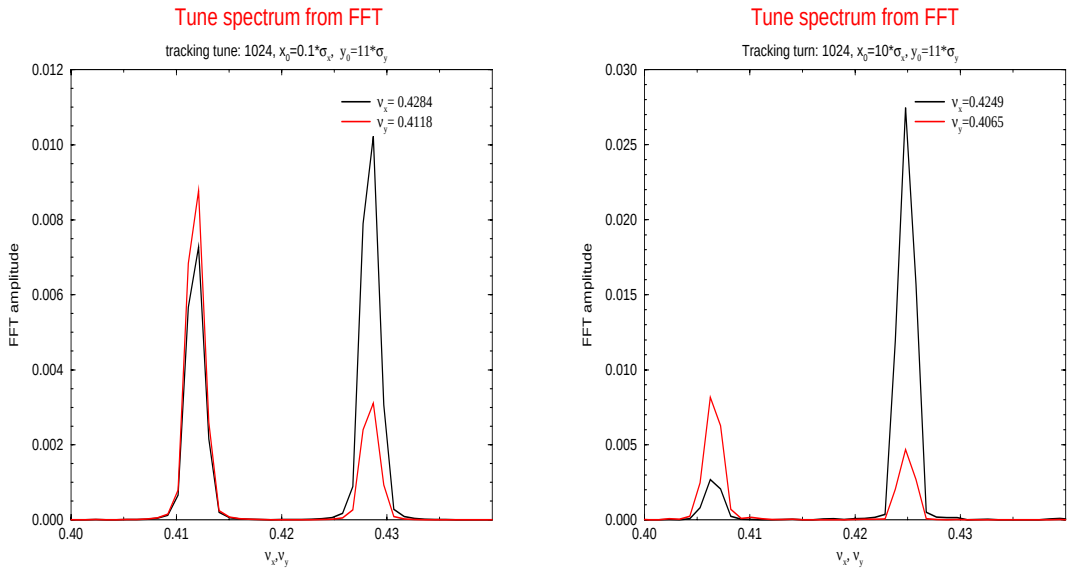

Figure 8: Tune spectrum of two particles at the same large y amplitude of $11\sigma_{y0}$ but at different x amplitudes of $0.1\sigma_{x0}$ (left figure) and $10\sigma_{x0}$ (right figure). Note that these particles with the same y amplitude have different vertical tunes because of the cross detuning. Coupling between the transverse planes can also be observed in the tune spectra of these particles.

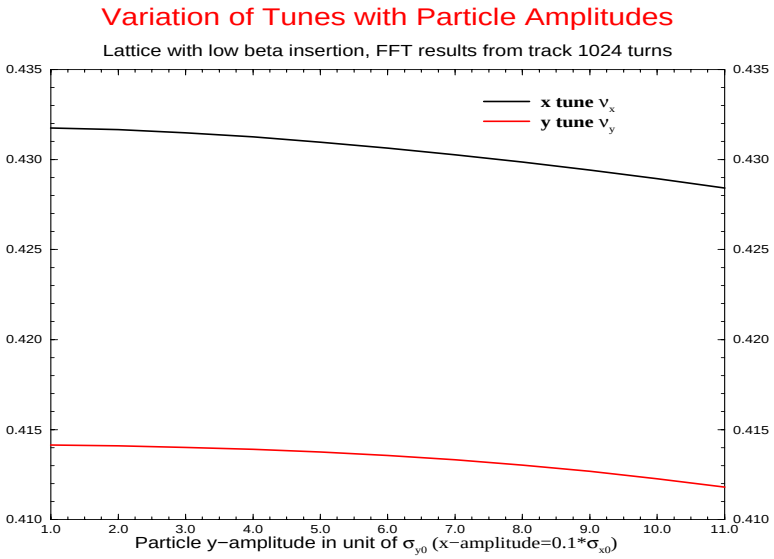

Figure 9: Variations of the horizontal and vertical tune with vertical amplitude - the horizontal amplitude is constant at $0.1\sigma_{x0}$. Note that at around $11\sigma_{y0}$, ν_x approaches the 7th order resonance.

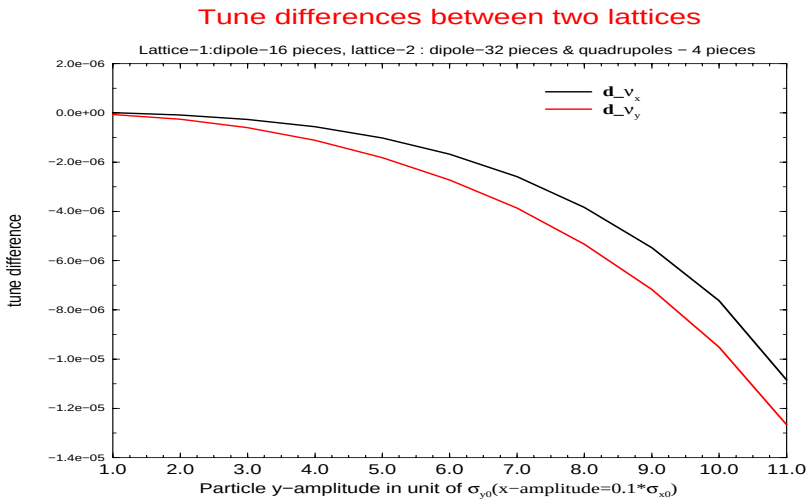

Figure 10: Tune difference between two lattices vs the particle amplitude. Lattice 1: dipoles split into 16 pieces, Lattice 2: dipoles split in 32 pieces, quadrupoles ino 4 pieces. The differences in tune are of the order of the resolution of the tune calculation.

6 Conclusion

This study of dynamic aperture in Recycler Ring with low beta straight section shows that the optical design of the low beta section improves the optical properties of the ring. Without misalignments, tracking calculations for on-energy particles over 10^5 turns predict a dynamic aperture of $16.5\sigma(817\pi mm.mrad)$ which is larger than the physical aperture of $47.625mm \times 22.225mm$. Misalignments will reduce this dynamic aperture but, if small enough, they should not limit the performance of the Recycler.

Acknowledgements

We thank Shekhar Mishra and David Johnson in the Recycler Ring department for providing the lattice and for their useful suggestions.

References

[1] G. Jackson, *The Fermilab Recycler Ring Technical Design Report*. Fermilab. November, 1996

[2] F. Christoph Iselin, *The MAD Program Physical Methods Manual*, Geneva, Switzerland. January 10, 1994

[3] T. Sen, unpublished notes

[4] S. Mishra, personal communication

Appendix A. The definition of a magnet as a beam line

Including high order multipole components, a magnet is defined by the following beam line,

A combined function dipole magnet = (DWELD, DEND, MP_N, MP_S, I …F(I …D), G_Body, O …F(O …D), MP_S, MP_N, DEND, DWELD)
A quadrupole magnet = (DWELD, QEND, QMP_N, QMP_S, Q_Body, QMP_S, QMP_N, QEND, DWELD)

where I . . . F(I . . . D) are the focusing and defocusing quadrupole components of combined function magnets, MP_N and MP_S are the integrated normal and skew components respectively of the nonlinear multipoles QMP_N and QMP_S are the integrated normal and skew components respectively of the nonlinear multipoles in the quadrupole magnet. DWELD and DEND are drift spaces.

A magnet after being split is defined as a beam line as follows:

A combined function dipole magnet = (DWELD, DEND, MP_N, MP_S, I …F(I …D), 16* G_Body_16, O …F(O …D), MP_S, MP_N, DEND, DWELD),

where G_body_16 is a piece with the length of $L/16$, L is the length of the gradient magnet.

Appendix B. Optics functions in Recycler Ring

.

Optical properties	Bare lattice	Lattice with all the errors	Lattice with all the errors gradient magnets split into 16 pieces
ν_x, ν_y	24.4062, 24.3933	24.4071, 24.3936	24.4071, 24.3936
$\nu_x^{'}, \nu_y^{'}$	-2.046, -2.736	-1.999, -2.709	-1.983, -2.770
$\beta_{x,max}, \beta_{y,max}$	243.496, 278.447	241.525, 277.744	241.521, 277.721
$D_x(max), D_y(max)$	2.152, 0.	2.159, 0.0806	2.159, 0.0806
$D_x(r.m.s.), D_y(r.m.s.)$	1.280, 0.	1.278, 0.0243	1.324, 0.0241
$x_{co}(max), y_{co}(max)$	0., 0.	1.970, 0.0407	1.970, 0.0407
$x_{co}(r.m.s.), y_{co}(r.m.s.)$	0., 0.	0.655, 0.0119	0.661, 0.0120

Table 2: Optical properties in the lattice with high beta straight section

Optical properties	Bare lattice	Lattice with all the errors	Lattice with all the errors gradient magnets split into 16 pieces $^{(*)}$
ν_x, ν_y	25.4289, 24.4158	25.4296, 24.4162	24.4297, 24.4162
$\nu_x^{'}, \nu_y^{'}$	-0.822, 0.327	-0.815, 0.347	-2.000, -2.000
$\beta_{xmax}, \beta_{ymax}$	71.123, 56.179	71.977, 56.049	72.243, 56.013
$D_x(max), D_y(max)$	2.144, 0.	2.164, 0.0785	2.159, 0.0786
$D_x(r.m.s.), D_y(r.m.s.)$	1.274, 0.	1.273, 0.0223	1.321, 0.0224
$x_{co}(max), y_{co}(max)$	0., 0.	1.902, 0.0372	1.903, 0.0372
$x_{co}(r.m.s.), y_{co}(r.m.s.)$	0., 0.	0.630, 0.0107	0.638, 0.0109

Table 3: Optical properties in the lattice with low beta straight section. *) The result in this column is the one after the adjustment of the strengths of chromaticity sextupoles in the arc cells.

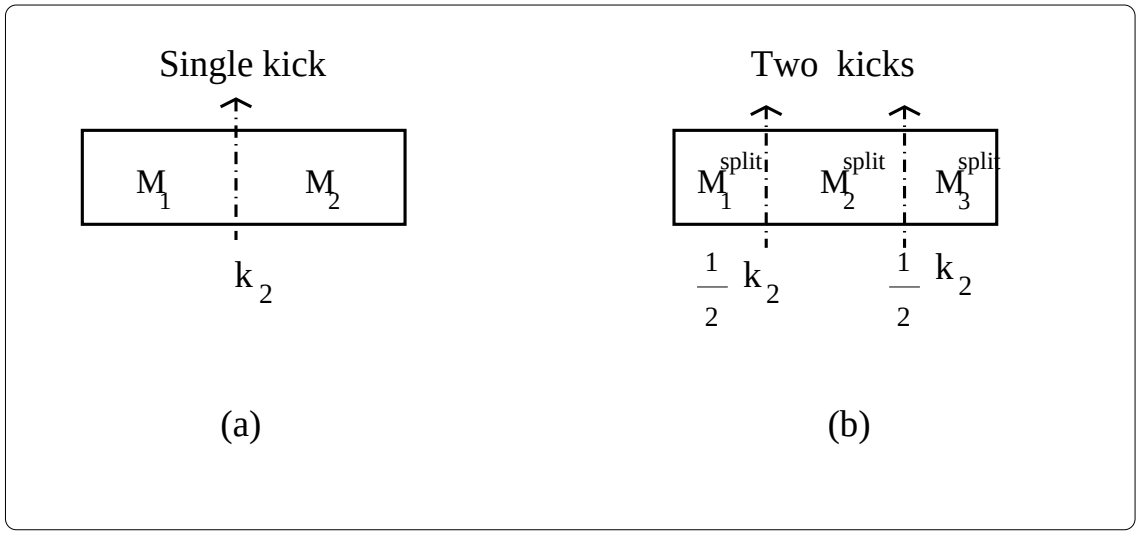

Figure 11: We compare the effect of a single kick acting at the center of a magnet (a) with that of two kicks (b), each of half the strength of the single kick in (a).

Appendix C. Amplitude change due to a single kick vs. due to two kicks.

Figure 11 shows a nonlinear kick at the center of a magnet and also two kicks each with half the strength of the single kick. For the purposes of illustration we will consider the nonlinear kick to be a sextupole kick of total integrated strength k_2 and evaluate the change in the linear Courant-Snyder invariant J_x after traversal through the magnet $GM328B$. With only a single kick at the center, the phase space variables are transported as

$$\begin{pmatrix} x \\ x' \end{pmatrix}_K^{before} = M_1 \begin{pmatrix} x \\ x' \end{pmatrix}_{in} \quad \text{before kick} \tag{9}$$

$$\begin{pmatrix} x \\ x' \end{pmatrix}_K^{after} = \begin{pmatrix} x_K^{before} \\ x_K^{'\,before} + k_2 (x_k^{before})^2 \end{pmatrix} \quad \text{after kick} \tag{10}$$

$$\begin{pmatrix} x \\ x' \end{pmatrix}_{out} = M_2 \begin{pmatrix} x \\ x' \end{pmatrix}_K^{after} \quad \text{at exit} \tag{11}$$

Then the linear invariant in the x plane at the exit of the magnet can be calculated as follows

$$J_1 = \frac{1}{2\beta_{x_{out}}} [x_{out}^2 + (\beta_{x_{out}} x_{out}^{'} + \alpha_{x_{out}} x_{out})^2] \tag{12}$$

We split $GM328B$ into two pieces as shown in Figure 11 (b). The kick strengths at each location are $k_2/2$. We do the same calculation as above and obtain the phase space variables at the magnet exit to be

$$\begin{pmatrix} x \\ x' \end{pmatrix}_{out}^{split} = M_3^{split} \begin{pmatrix} x \\ x' \end{pmatrix}_{2nd\ kick}^{after} \tag{13}$$

Distance in the lattice (m)	Single kick			Two kicks		
	β (m)	α (1)	ν(2 π)	β (m)	α (1)	ν(2 π)
0.609	42.938	0.026	0.002	42.938	0.026	0.002
1.733				42.429	0.542	0.006
2.857	40.525	1.026	0.011	40.525	1.026	0.011
3.981				37.726	1.453	0.015
5.105	34.057	1.796	0.020	34.057	1.796	0.020

Table 4: Twiss functions in Magnet GM328B in the lattice with high beta insertion.

Initial (x, x')	Linear Invariant J	
	Single kick: J_1	Two kicks: J_2
(3.88, 0.)	0.25277	0.24768
(3.88, 0.01)	0.23291	0.22931

Table 5: Linear invariants at the exit of Magnet GM328B

and the linear invariant in the x plane this case is

$$J_2 = \frac{1}{2\beta_{x_{out}}}[(x_{out}^{split})^2 + (\beta_{x_{out}} x_{out}^{'\ split} + \alpha_{x_{out}} x_{out}^{split})^2] \tag{14}$$

The beta functions at each location in the magnet, listed in Table 4, are taken from the beam line in the lattice with high beta section, and are used to calculate the transfer matrices M_1, M_2, ..., M_3^{split}. With two kicks per magnet, there is a phase difference of about 3 degrees between the kicks. In itself this is not large but this is repeated in every magnet and these small changes can lead to significant differences in amplitude after several turns.

We have calculated the quasi-invariants, J_1 and J_2, at the exit of magnet $GM328B$ after a single pass for two different initial conditions. The linear invariants in these two cases are shown in Table 5. We observe that in both cases $J_2 < J_1$. This demonstrates that the combined effect of two slightly incoherent kicks leads to a smaller change in amplitude compared to a single kick of the same total integrated strength. As argued in Section 5 we expect the change in amplitude to decrease as the number of kicks is increased before reaching an asymptotic limit.